

# Performance of 1-mm<sup>2</sup> Silicon Photomultiplier

A. G. Stewart, V. Saveliev, S. J. Bellis, D. J. Herbert, P. J. Hughes, and J. C. Jackson

**Abstract**—A silicon photomultiplier (SPM) is a large area detector consisting of a parallel array of photon counting microcells. Each microcell consists of a Geiger Mode photodiode with an integrated quenching element. Each microcell is then connected to a common output. The microcells have a uniform gain of up to 10<sup>6</sup> and provide an identical charge output signal for each photon detected. Under illumination the summed output of the detector is proportional to the number of Geiger pulses and hence proportional to the incident photon flux. This combination gives extremely high performance comparable to that of a conventional photomultiplier tube (PMT). We report on the characterization of two different 1 mm<sup>2</sup> SPM detector designs with 620 and 920 microcells at room temperature (20 °C) and down to −30 °C. We assess detection efficiency, breakdown voltage, gain, dark rate, crosstalk, timing jitter and dynamic range. The SPM detector operates over the visible region of the spectrum, characterized here from 400 to 800 nm. The peak photon detection efficiency of 15% occurs at 500 nm with a cooled (−20 °C) dark rate of 600 kHz/mm<sup>2</sup> at a bias voltage of 31 V. In a test for positron emission tomography (PET), an energy resolution of 25% was recorded for the detection of 511 keV gamma radiation using 1 mm × 1 mm × 15 mm LYSO scintillator crystal. The SPM has many applications such as medical imaging, microscopy, high-energy physics, and homeland security.

**Index Terms**—Geiger mode photodiodes, photomultiplier tube (PMT), positron emission tomography (PET), scintillation detectors, silicon.

## I. INTRODUCTION

ORIGINALLY developed in Russia in the mid-1980s, silicon photomultiplier (SPM) detectors have received considerable research effort over the past 10 years and the technology is now maturing [1]–[5]. The performance of SPM detectors is fast approaching that of conventional photomultiplier tube (PMT) detectors and is superior to that of linear mode avalanche photodiode (APD) detectors in terms of sensitivity, noise and gain. In addition, SPM detectors have a number of advantages over PMT detectors including; small size, low bias voltage operation, magnetic field insensitivity, a higher degree of robustness and immunity to damage from high light condition overexposure. The SPM also takes advantage of the high degree of fabrication uniformity afforded by fabrication in a modern batch processed semiconductor fabrication facility.

Manuscript received August 1, 2007; revised September 7, 2007.

A. G. Stewart is with SensL, Blackrock, Cork, Ireland (e-mail: astewart@sensl.com).

V. Saveliev is with Obninsk State University, Obninsk, Russia and also with DESY, 22607 Hamburg, Germany (e-mail: saveliev@mail.desy.de).

S. J. Bellis, D. J. Herbert, P. J. Hughes, and J. C. Jackson are with SensL, Blackrock, Cork, Ireland (e-mail: sbellis@sensl.com; dherbert@sensl.com; phughes@sensl.com; cjackson@sensl.com).

Color versions of one or more of the figures in this paper are available online at <http://ieeexplore.ieee.org>.

Digital Object Identifier 10.1109/JQE.2007.910940

The SPM output signal to a fast, low intensity optical pulse is an integer number of Geiger pulses proportional to the incident pulse intensity. The high internal amplification or gain of the Geiger pulses is uniform and fixed and not determined by statistics of the multiplication process as is the case for linear mode APD detectors. As a result, the concept of multiplication or excess noise is not relevant and the output of the SPM is an identical charge pulse for every photon detected. This uniformity in gain across the SPM gives exceptional photon counting performance and the ability to resolve the single photoelectron spectrum.

Applications particularly suited to SPM technology include scintillator read-out for high-energy physics and nuclear medicine, including positron emission tomography (PET) and single photon emission computed tomography (SPECT), microscopy and radiation detection for homeland security systems [6].

## II. SILICON PHOTOMULTIPLIERS

### A. Concept

The core of an SPM is a silicon photon counting diode [7]. These photon counting diodes are designed to operate above breakdown voltage in a mode of operation known as Geiger mode. In Geiger mode, photons entering the photodiode generate a self-sustaining avalanche current which is quenched and reset by use of either passive elements [8] or active quenching circuits [9]. The limitation of a photon counting detector is the need for it to quench and reset after every photon event. Practically, this limits the maximum count rate to 10 MHz. Additionally, a photon counting detector is a binary device that is either on or off. The binary nature is exploited for photon timing; however, the output is independent of the number of simultaneous incident photons [10]. A photon counting diode cannot distinguish between multiple photons incident on the detector at the same time. To overcome this limitation a parallel array of photon counting diodes, Fig. 1, can be implemented such that the output becomes proportional to the incident photon flux. The high performance of the SPM results from new integration concepts and modern semiconductor fabrication techniques. These techniques allow the fabrication of arrays of Geiger mode photodiodes, where each photodiode is coupled to an integrated quench element to form the SPM microcell.

### B. SPM Design and Fabrication

The SPM detectors measured in this study were fabricated on silicon epitaxial p-type wafers. The microcells are formed from planar n<sup>+</sup>-p junctions. An implanted p<sup>+</sup> layer forms an enrichment region that defines the active area and breakdown voltage of the junction. The n<sup>+</sup> top contact layer is formed by diffusion of n-type dopant implanted in polysilicon. The n<sup>+</sup> layer overlaps

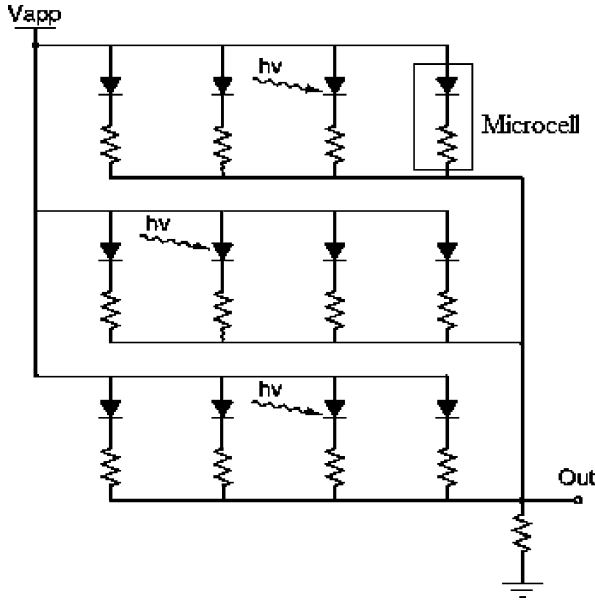


Fig. 1. Schematic diagram of an SPM.

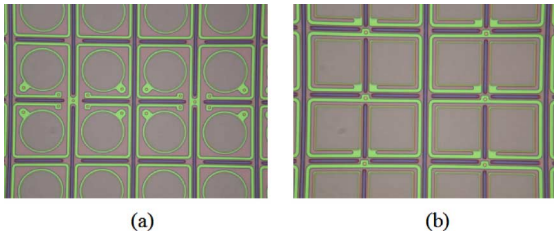


Fig. 2. Micrograph of the design layout of the two SPM detectors investigated in this work. (a) SPM1. (b) SPM2.

the enrichment region to form a virtual guard ring. The virtual guard ring reduces the electric field at the edge of the diode and allows a uniform breakdown region [11]. The polysilicon layer extends beyond the active area of the diode and is implanted to produce a resistor on the order of hundreds of kilo-ohms. The formation of the quench resistor and the connection to the output node reduce the fill factor of the SPM. There is a fundamental tradeoff between the size of the microcell active area, the number of microcells and the fill factor for a given SPM geometry.

To investigate these tradeoffs, the characteristics of two SPM designs are reported. The geometry and layout of the microcells in the two designs are shown in Fig. 2. The area between microcells is not optically sensitive and the ratio of optically sensitive to insensitive silicon defines the SPM geometrical efficiency or fill factor. In the first design, SPM1, the microcells have a circular geometry with an active area diameter of  $20\ \mu\text{m}$  on a  $42\text{-}\mu\text{m}$  pitch. SPM1 consists of 620 microcells and has a fill factor of 17%. In the second design, SPM2, the microcells are square with length  $20\ \mu\text{m}$  with rounded corners on a  $32\text{-}\mu\text{m}$  pitch. SPM2 has 920 microcells and a fill factor of 34%. The main design parameters are summarized in Table I.

### III. SPM CHARACTERIZATION

#### A. Photon Detection Efficiency

The photon detection efficiency (PDE) of an SPM is determined by three parameters; quantum efficiency, geometrical ef-

TABLE I  
DESIGN PARAMETERS OF SPM DETECTORS

| Design | Microcell Geometry        | Microcell Size              | Number of Microcells | Fill Factor |
|--------|---------------------------|-----------------------------|----------------------|-------------|
| SPM1   | Circle                    | $20\ \mu\text{m}$ Diameter  | 620                  | 17.8%       |
| SPM2   | Square with round corners | $20 \times 20\ \mu\text{m}$ | 920                  | 34.2%       |

iciency and avalanche initiation probability (AIP). The PDE is given by

$$\text{PDE}(V, \lambda) = \eta(\lambda) \cdot \varepsilon(V) \cdot F \quad (1)$$

where  $\eta(\lambda)$  is the silicon quantum efficiency,  $\varepsilon(V)$  is the avalanche initiation probability and is a function of the bias voltage and  $F$  is the SPM geometrical efficiency.

The quantum efficiency of silicon is 80+% over much of the visible spectrum, 400–700 nm [12]. The bandgap of silicon limits the operating wavelength to less than  $1.1\ \mu\text{m}$  while surface reflections and junction depth limit the detection of photons below 400 nm. At 400 nm, for example, the majority of photons are absorbed within 100 nm of the surface. If the junction depletion region is more than 100 nm below the surface then these photo-carriers have a reduced probability of being detected.

The geometrical efficiency is defined as the ratio of the total active area of all the SPM microcells to the total area of the SPM. The avalanche initiation probability is the probability that a carrier in the depletion region initiates a Geiger avalanche and is a function of the bias voltage. Not every photo-generated carrier will succeed in generating a Geiger avalanche. There is a nonzero probability that the seed carrier will lose energy to phonon interactions and recombine such that the chain of ionizations stop before the entire junction goes into Geiger breakdown. The avalanche initiation probability can be calculated provided the electric field profile and the electron and hole ionization coefficients are known [13].

The direct measurement of the SPM PDE is complicated by two effects; optical crosstalk and after-pulsing. Afterpulsing is the generation of false counts that arise from the emission of carriers that were trapped in bandgap states in the depletion region during previous Geiger events [14]. Optical crosstalk occurs when a photon, emitted by the avalanching carriers in one microcell, travels to a neighboring microcell and initiates an avalanche breakdown [15]. Optical crosstalk is discussed further in Section III-E. Both these processes result in additional Geiger pulses and result in an over estimation of the SPM PDE.

#### B. Linearity and Dynamic Range

The detection of photons by an SPM is a statistical process based on the probability of detecting randomly distributed photons by the limited number of sensitive elements. The SPM PDE and the total number of microcells determine the dynamic range of the SPM. The number of microcells fired as a function of the number of incident photons can be approximated by the following expression

$$N_{\text{Fired}} = M \left( 1 - \exp \left( -\frac{\text{PDE} \cdot N_{\text{Ph}}}{M} \right) \right) \quad (2)$$

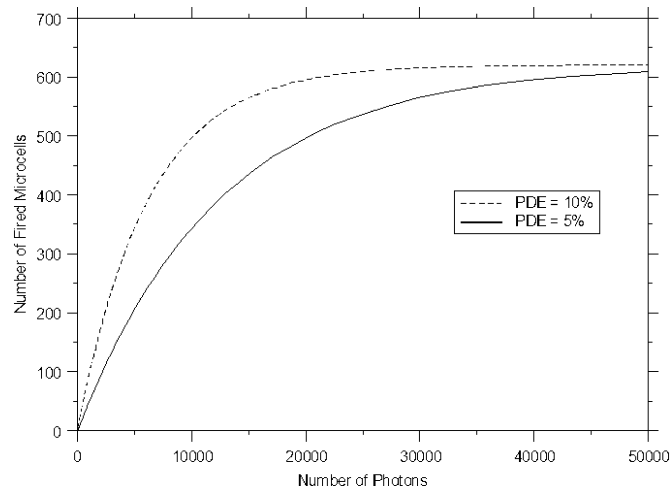


Fig. 3. SPM response as a function of the number of instantaneous photons for two different PDE values. The solid curve shows the response of an SPM with 5% PDE while the dashed curve shows the SPM response for an SPM with 10% PDE.

where  $M$  is the total number of microcells in the SPM,  $N_{Ph}$  is the number of instantaneous photons,  $PDE$  is the SPM photon detection efficiency and  $N_{Fired}$  is the number of microcells fired by the incident photons. Fig. 3 shows the detector response (number of microcells fired) as a function of the number of instantaneous incident photons for an SPM with 620 microcells and with a PDE of 5% and a PDE of 10%. The SPM response is linear when the number of incident photons is much less than the total number of cells. The SPM response becomes sub-linear when the number of microcells fired reaches approximately a quarter of the total number of microcells.

The figure also shows how the SPM dynamic range and linearity can be extended to handle higher photon fluxes by lowering the operating bias and hence reducing the SPM PDE, in this example, from 10% to 5%.

### C. Timing

The Geiger pulse timing characteristics are defined by two parameters; the onset time and the recovery time. The onset time is defined by the diode discharge time. The recovery time is defined by the  $RC$  combination of the quench resistor, diode capacitance and external circuitry. The true onset time of the Geiger pulse is difficult to measure without fast amplifiers and electronics, it is estimated to be on the order of hundreds of picoseconds [16].

The time resolution of the SPM is dictated by the timing jitter of the microcells. The timing jitter is the statistical variation in the time between the arrival of an optical pulse at the SPM and the subsequent electrical signal response from the SPM. The timing jitter arises from a number of processes. Firstly, the transmitted optical pulse has a finite rise time and duration. The probability of detecting a photon during the optical pulse lifetime is a statistical process. Hence, the statistical variation in detection and optical pulse lifetime will add to the time jitter. Secondly, the Geiger avalanche processes requires a finite time to reach its resistance limited value and variations in this avalanche time also adds to the timing jitter. The Geiger avalanche time will

also have a time jitter due to the spatial variation in the location where the photo-carriers are first generated. The spatial variation can be lateral across the photodiode or in the vertical direction. The penetration depth for the photons is a function of wavelength and the statistical probability that a photon is absorbed close to the junction decreases with increasing wavelength.

### D. Dark Rate

One of the main factors limiting the performance of the SPM is the dark rate. The dark rate results from thermally generated carriers that can also initiate a Geiger avalanche that results in a current pulse that is indistinguishable from a pulse produced by the detection of a photon. This is particularly important for room temperature operation. The SPM dark rate is the average frequency of the thermally generated Geiger avalanches from all the microcells in the array. In many applications the average dark rate can be measured and subtracted. However, the statistical variation in the dark rate cannot be subtracted and constitutes a noise source that determines the minimum detectable signal.

### E. Optical Crosstalk

When undergoing Geiger avalanche, carriers near the junction emit photons as they are accelerated by the high electric field [17]. The photons emitted are spread across the visible spectrum and typically  $2 \times 10^{-5}$  photons are emitted per electron crossing the junction [18]. These photons can travel to neighboring microcells and initiate a Geiger avalanche in one or more of the neighboring microcells. This process is known as optical crosstalk.

The crosstalk probability is the probability that an avalanching microcell will trigger a second microcell to avalanche. The process happens practically instantaneously and results in an output pulse with twice the charge or twice the amplitude of a Geiger pulse from a single microcell. The optical crosstalk probability is a function of SPM bias voltage and the distance between neighboring microcells. However, the crosstalk can be significantly reduced by optically isolating the microcells from each other. This can be achieved by etching a trench between the microcells and filling it with an optically opaque material.

### F. Afterpulsing

Afterpulsing is the name given to Geiger pulses that occur after and are correlated to a random dark or photon initiated Geiger pulse. Afterpulsing occurs due to the release of carriers captured by traps during a Geiger avalanche. During a Geiger avalanche, a large number of mobile carriers cross the junction. When this occurs there is a finite probability that a carrier may become trapped by a bandgap state. The carrier may then be released at some later time and trigger a new Geiger avalanche event.

Afterpulsing is described in terms of a probability. The afterpulsing probability is the probability that any given pulse is followed by a false count or afterpulse. The afterpulsing probability is a function of the mean lifetime of the carrier in the trap. The trap lifetime depends on the trap properties, the type of carrier trapped and the temperature. Short trap lifetimes result

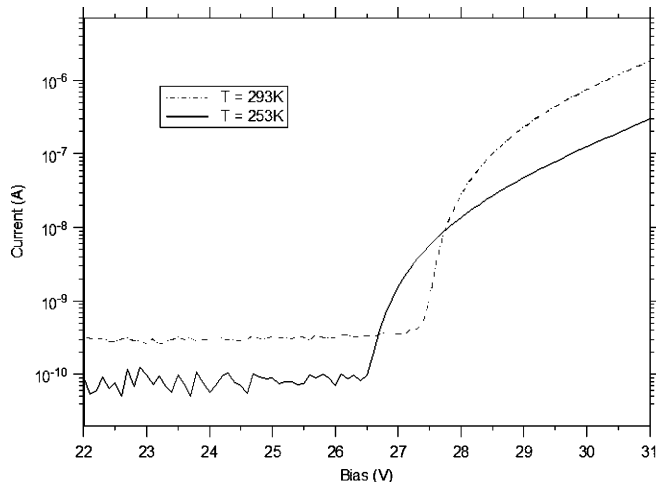


Fig. 4. Typical reverse  $I$ - $V$  characteristics of SPM2 at room temperature and at 253 K.

in a low afterpulsing probability since the carriers are likely to be emitted before the diode has fully recovered and the carrier avalanche initiation probabilities are low. Afterpulses occurring before the diode has fully recovered will also have a lower gain since the diode will not have fully recharged.

#### IV. EXPERIMENTAL RESULTS

##### A. IV Characteristics

Fig. 4 shows the typical reverse bias IV characteristics for SPM2 at room temperature and at 253 K ( $-20^{\circ}\text{C}$ ). The SPM IV characteristic is used to determine the breakdown voltage of the microcells. The breakdown voltage is a function of temperature and has a temperature coefficient of  $23\text{ mV}/^{\circ}\text{C}$ .

##### B. Photon Detection Efficiency

To eliminate the effect of crosstalk, the PDE has been determined by measuring the photon detection probability (PDP) of individual Geiger mode photodiodes identical to those contained within the SPM array. The individual photodiodes do not contain the integrated resistor of the SPM microcell. The PDP is defined as the quantum efficiency of silicon times the carrier avalanche initiation probability (AIP). The SPM PDE is then determined by scaling the PDP with the geometrical efficiency. This method contains the afterpulsing in the microcell but eliminates the optical crosstalk as a positive contributor to the PDE, which it is not.

The Geiger mode photodiode PDP was measured relative to a calibrated 1853-C Newport detector. The microcell and Newport detector are attached to adjacent ports of an integrating sphere and illuminated with a low level continuous signal from a Bentham TMc300 monochromator and white light source through a third port in the integrating sphere. The dark current and photocurrent are then recorded at each wavelength along with the photon flux incident on the reference detector. The photodiode PDP was recorded using both active and passive quenching circuits and the photon flux was kept below 100 kcps

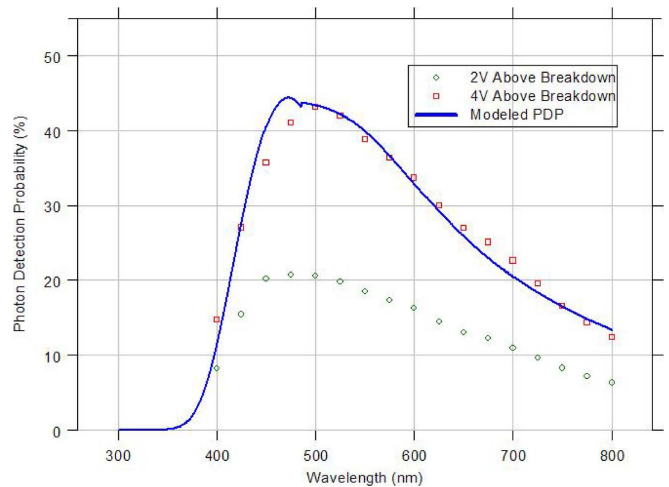


Fig. 5. Photon detection probability of a single Geiger mode APD identical to those contained within the SPM. The PDP was measured at 2 V (circles) and 4 V (squares) above the breakdown voltage. The spectral response of the detector can be modeled using an absorption probability distribution and the spectral transmittance of the antireflection coating. A fit to the PDP data is obtained using the avalanche initiation probability (AIP) of the carriers as a fitting parameter.

to prevent saturation of the photodiode. The PDP was found to be similar for both quenching methods.

Fig. 5 shows the measured photodiode PDP as a function of wavelength at 2 and 4 V above the breakdown voltage together with the predicted wavelength response. At 4 V above breakdown the peak PDP is 43% and occurs at 500 nm. At 2 V above breakdown, the peak PDP shifts to a slightly lower wavelength and has a peak value of 21%. Scaling the photodiode PDP with the SPM fill factor gives the SPM PDE. SPM1, which has a low fill factor, will therefore have a PDE of 8% at 4 V above breakdown while SPM2 will have a peak PDE of 15% at 4 V above the breakdown voltage.

The PDP was modeled using the absorption coefficient of silicon and the probability that a photon will be absorbed in the depletion region together with a model of the transmittance of the SPM antireflection coating. The depletion layer absorption and antireflection coating determine the spectral profile of the PDP which is then scaled to fit to the experimental PDP data by using the AIP as a fitting parameter.

##### C. Single Photoelectron Spectrum

The stable, high gain of the Geiger mode photodiodes within the SPM mean that minimal electronics are required to observe the signal pulses. With a simple low gain amplifier the Geiger pulses can be observed on an oscilloscope or read into a charge integrating ADC.

Fig. 6 shows the Geiger pulses as viewed on an oscilloscope,  $50\ \Omega$  input impedance, with an ac-coupled amplifier with a gain of 1500. The first two Geiger pulses are the result of single microcells avalanching while the third pulse, which has an amplitude twice that of a single Geiger pulse, is the result of two microcells firing simultaneously (optical crosstalk). The peak height of the single Geiger pulses is commonly referred to as the single photoelectron level. Likewise, a pulse with a peak height

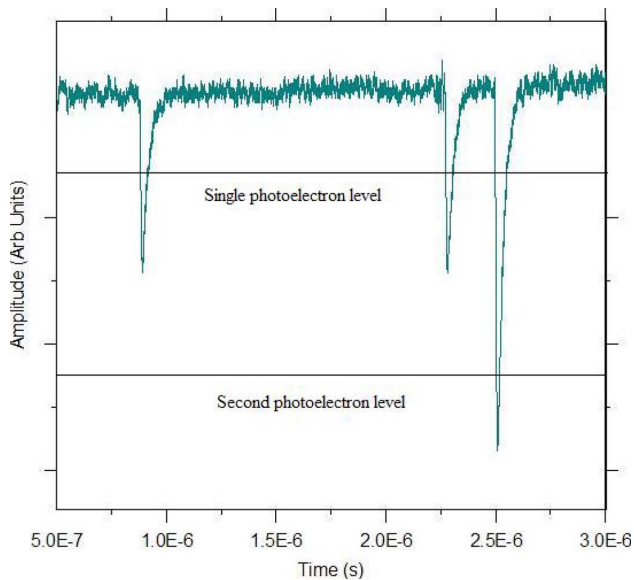


Fig. 6. SPM response as viewed on an oscilloscope. Two single level Geiger pulses and a pulse with twice the amplitude of a single pulse are shown. The single level pulses define the single photoelectron level. When two or more pulses occur simultaneously, for example due to crosstalk or an optical pulse, the Geiger pulses superimpose producing a pulse with an amplitude equal to a multiple of the single pulse amplitude.

2, 3 and so on, times the amplitude of a single Geiger pulse are referred to as the second and third photoelectron level.

The pulse timing characteristics, as measured by the oscilloscope, are a convolution of the microcell time response and the readout electronics bandwidth. The onset or fall time of Geiger pulses shown in the figure is 6–7 ns while the recovery time is 45–60 ns.

A histogram of the ADC output in response to repeated fast pulses of low-level light incident on the SPM results in a photoelectron spectrum with well-resolved peaks. Such a spectrum is indicative of the low noise and uniform stable gain of the Geiger mode photodiodes. Fig. 7 shows the single photoelectron spectrum (SPS) from SPM1. To obtain the spectrum, the charge from the SPM is integrated for a fixed gate time. The gate width should be of the order of the full width of the Geiger pulses and is typically around 100 ns. The integration window is set to coincide with a very fast optical pulse ( $\ll 100$  ns). In this way, the charge from 1 to  $n$  microcells, where  $n$  is the number peaks in the spectrum, can be measured with minimal interference from noise sources such as the dark pulses. The first peak in the spectrum, often called the pedestal, is a measure of the noise in the system (detector + electronics) and corresponds to instances when no Geiger pulses were recorded during the gate time, i.e., no photons detected. The second peak of the spectrum, or the first photoelectron peak, corresponds to a single microcell firing during the gate time. Subsequent peaks correspond to two, three, four and so on microcells firing during the gate time. The peaks are well resolved demonstrating the excellent photon counting properties of the SPM.

#### D. Afterpulsing

As with the PDP, the afterpulsing probability is measured on a single Geiger mode photodiode identical to those contained

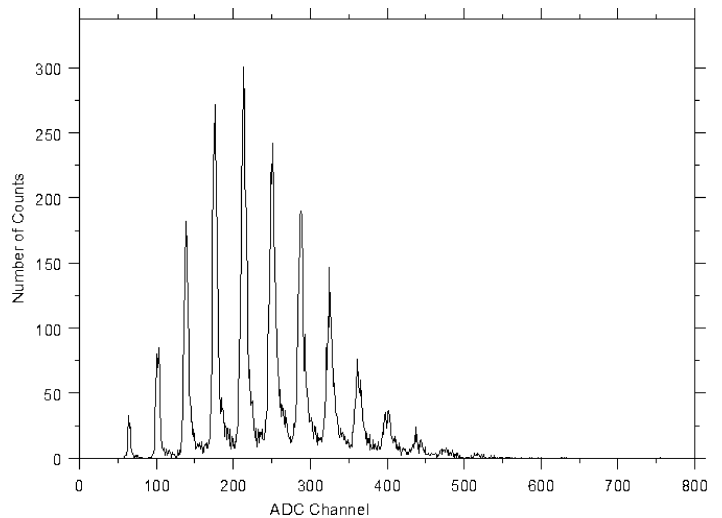


Fig. 7. Single photoelectron spectrum from SPM1 at room temperature.

in the SPM. The afterpulsing probability was measured using a Becker and Hickl SPC140 time correlated single photon counting (TCSPC) PC card and a 650-nm laser and active quenching. The laser fires 47-ps pulses at a repetition rate of 50 MHz onto the detector surface and neutral density filters are used to adjust the count rate to 100 kHz. The TCSPC card then determines the correlation of pulses, which is converted via data processing to the afterpulse probability [19]. The Geiger mode photodiodes were found to have an afterpulsing probability of 0.3% at 2 V above the breakdown voltage and 8% at 4 V above the breakdown voltage. The measured afterpulse probability depends on the quenching method and while the quench/recovery time of the active quench measurement on the Geiger photodiode was set to be similar to that of the SPM microcell further work is required to establish if the afterpulse probability of the Geiger photodiodes is different in the passive quench configuration of the SPM microcell.

Afterpulsing adds false counts to the measurement of an optical signal and should be corrected for to obtain an accurate measurement of an incident photon flux. In an SPM PDE measurement, the PDE will be over estimated if an afterpulse correction is not taken into account.

#### E. Timing Jitter

The timing jitter spectrum for SPM2, shown in Fig. 8, was obtained using a 650-nm laser source and a Becker and Hickl TCSPC PC card. In this case the laser source was a Firecomms (RVM665T) VCSEL driven with short 430-ps electrical pulses from a HP8131A pulse generator. The pulse generator also supplies the trigger to start the time measurement. The jitter histogram is fitted with a Gaussian curve and has a FWHM of 65 ps and represents the jitter from the system including the VCSEL and jitter from the pulse generator. A similar result was obtained from SPM1.

#### F. SPM Microcell Gain

The SPS also allows the gain of the microcells and the gain uniformity to be determined. The gain is given by the separation of the peaks and is defined as the charge generated by a Geiger

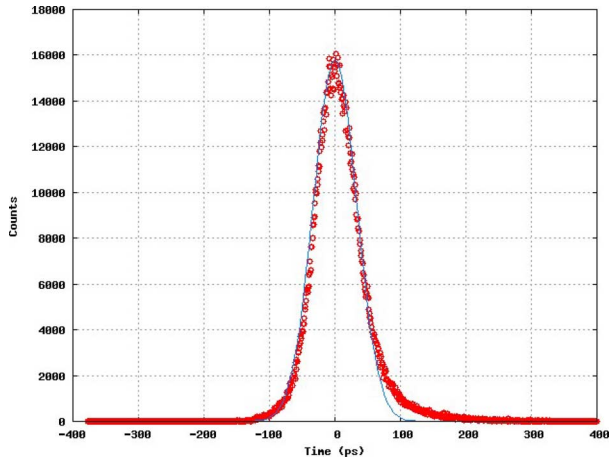


Fig. 8. Jitter histogram from SPM2 with fitted Gaussian curve. The FWHM is 65 ps.

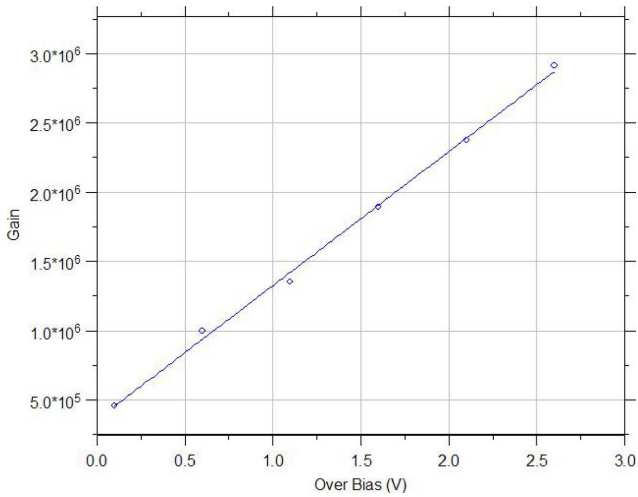


Fig. 9. SPM microcell gain as a function of over-bias.

avalanche event divided by the charge on an electron. The gain is a function of detector bias and temperature. The intra and intermicrocell gain variation can be determined from the FWHM of the photoelectron peaks

Fig. 9 shows the microcell gain increases linearly with detector bias and is greater than  $1 \times 10^6$  at 0.7 V above the breakdown voltage. A similar dependence and gain value was found for SPM1.

### G. Dark Rate Measurement

The dark rate was recorded using the counter function on a 54641A Agilent oscilloscope. The counter function counts trigger level crossings and displays the result in Hz. The dark rate is a function of the trigger level and to record the rate of single level Geiger pulses the trigger level was set at half the peak height of the single Geiger pulses.

Fig. 10 shows the dark rate as a function of over-bias for SPM1 and SPM2 at room temperature and at  $-20^\circ\text{C}$ . At room temperature the dark rate increases linearly at a rate of 0.95 MHz/V for the SPM1 design and 1.67 MHz/V for the SPM2 design.

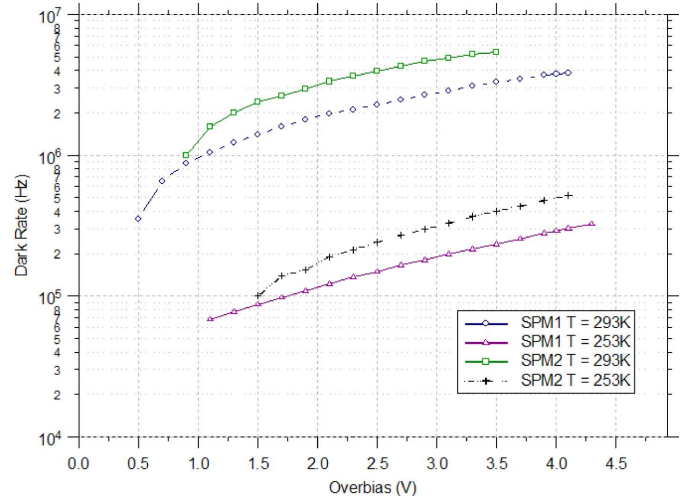


Fig. 10. Dark rate as a function of over-bias for SPM1 and SPM2 at room temperature and at  $253\text{ K } (-20^\circ\text{C})$ .

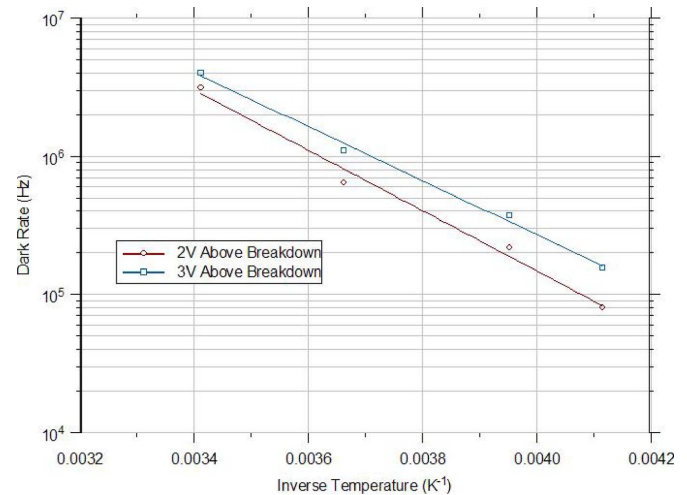


Fig. 11. Arrhenius plot of SPM2 dark rate at 2 and 3 V above the breakdown voltage. The activation energy is 433 meV at 2 V above breakdown.

As the dark rate at room temperature is thermally activated it is a strong function of temperature. Fig. 11 shows an Arrhenius plot of the dark rate of SPM2 at 2 and 3 V above the breakdown voltage. The plot gives a dark rate thermal activation energy of 433 meV at 2 V above breakdown and 388 meV at 3 V above breakdown. These activation energies are close to half the bandgap of silicon (560 meV) and are indicative of thermal generation from a single trap level in the depletion region [20].

### H. Optical Crosstalk

The optical crosstalk probability can be estimated by the ratio of the count rate at the second photoelectron level to the count rate at the single photoelectron level. The count rate at the single photoelectron level is measured by setting the threshold at half the peak height of the Geiger pulses while the rate at the second photoelectron level is measured by setting the threshold at 1.5 times the Geiger pulse peak height. The measurements were taken at 253 K to reduce the primary dark rate. At room temperature were the dark rates are of the order of megahertz, there

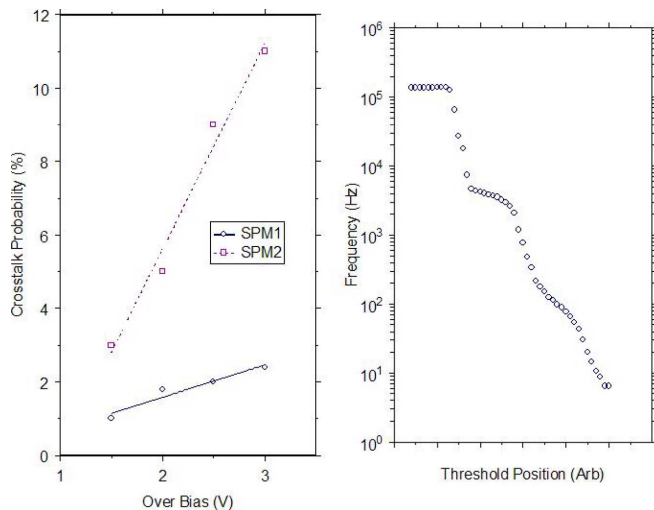


Fig. 12. Crosstalk probability as a function of over-bias for SPM1 and SPM2 at 253 K (left) and pulse frequency as a function of threshold position at 3 V over-bias and at 253 K for SPM1 (right).

is a higher probability that two uncorrelated dark pulses or a dark pulse and an afterpulse event might coincide to produce a pulse with amplitude greater than the threshold setting for the second photoelectron level. At 253 K, the primary dark rate is of the order of a few hundred kilohertz and the probability of uncorrelated events occurring simultaneously is reduced.

Fig. 12 shows the crosstalk probability, measured at 253 K, for SPM1 and SPM2 as a function of over-bias (left) and the pulse frequency as a function of threshold level for SPM1 (right).

The crosstalk probability increases linearly with over-bias and, as expected, the SPM2 design has a higher crosstalk probability as the microcell pitch in this design is smaller. Plotting the pulse frequency as a function of threshold position produces a step-like curve. The flat regions of the curve correspond to the frequency of pulses at the single, double, triple photoelectron level. In the example shown the pulse frequency was measured at 253 K and at 3 V over-bias. At a low threshold, the frequency corresponds to the single photoelectron level rate or dark rate of the SPM. As the threshold increases above the peak height of the single Geiger pulses, the rate falls as only pulses at the second photoelectron level, i.e., crosstalk, will now be measured. The rate then remains constant until the threshold increases above the peak height of two coincident pulses and then falls to the rate of the third photoelectron level. Pulses at the third photoelectron level are also mostly due to crosstalk. However, for many applications the importance of this measurement shows that by setting the threshold level to higher than a single photoelectron pulse, it is possible to remove most of the dark count signal and predominantly view pulses of 2 or more photons per pulse with a low dark count.

## V. APPLICATION

An important area of application for SPM technology is in imaging systems for nuclear medicine, in particular PET. The main goal of the photodetector in PET imaging is the fast and

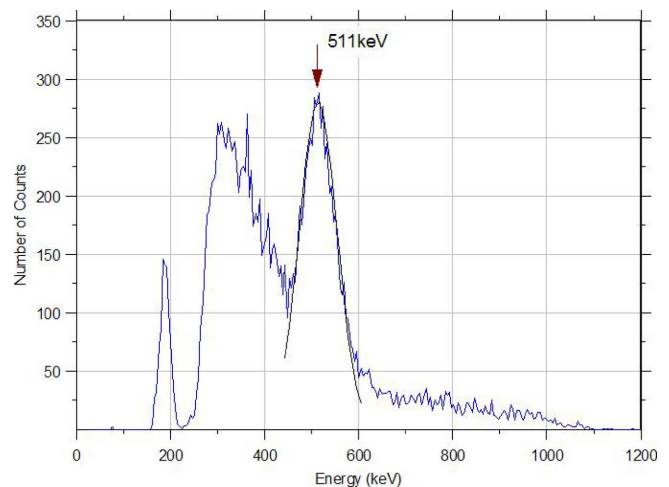


Fig. 13. Energy spectrum for 511 keV gamma radiation using an LYSO/SPM2 detection system. A fit to the 511 keV peak gives a resolution of approximately 25%.

efficient detection of 511 keV gamma rays from positron annihilation.

Fig. 13 shows the room temperature spectra acquired from the detection of 511-keV gamma rays from a <sup>22</sup>Na source by a 1 mm × 1 mm × 15 mm LYSO scintillator crystal directly coupled to a 1 mm × 1 mm SPM with SPM2 design. The SPM output was recorded on an ADC with self-triggering. A fit to the 511 keV peak gives an energy resolution (full-width at half-maximum) of approximately 25%. In this measurement the coupling between the scintillator and the SPM was not ideal resulting in a reduced energy resolution due to the poor light collection efficiency. With better coupling between the scintillator and SPM the energy should improve significantly. For example, recent energy spectra obtained using a 9 mm<sup>2</sup> SPM detector have achieved an energy resolution of 12.5% for LYSO at 511 keV.

## VI. CONCLUSION

The principle performance parameters of 1 mm<sup>2</sup> SPM detectors based on a CMOS compatible process have been characterized. These include the PDE, dark rate, gain, time resolution and crosstalk. Two designs of SPM have been characterized and the results show that while increases in fill factor provides a higher PDE for the SPM, there is a corresponding increase in crosstalk and dark counting rate. Both designs were found to have fast pulse onset times and have uniform, high gain (> 10<sup>6</sup>).

The dark rate has been shown to be thermally activated with a temperature dependence similar to the intrinsic carrier concentration  $n_i$ . This is indicative of a depletion layer generation current due to a trap level.

The detectors have applications in high-energy physics and nuclear medicine for scintillator read-out, fluorescence detection and in a multitude of other low-light level applications where linear mode APD and PMT detectors are currently used.

## REFERENCES

- [1] V. Saveliev and V. Golovin, "Silicon avalanche photodiodes on the base of metal-resistor-semiconductor (MRS) structures," *Nucl. Instr. Meth. A*, vol. 442, no. 1-3, pp. 223–229, Mar. 2000.

- [2] G. Bondarenko *et al.*, "Limited Geiger-mode microcell silicon photodiode: New results," *Nucl. Instr. Meth. A*, vol. 442, pp. 187–192, 2000.
- [3] A. G. Stewart, E. Green-O'Sullivan, D. J. Herbert, V. Saveliev, F. Quinlan, L. Wall, P. J. Hughes, A. Mathewson, and J. C. Jackson, in *Proc. SPIE, Study of the Properties of New SPM Detectors*, 2006, vol. 6119, pp. 84–93.
- [4] V. Golovin and V. Saveliev, "Novel type of avalanche photodetector with Geiger mode operation," *Nucl. Instr. Meth. A*, vol. 518, pp. 560–564, 2004.
- [5] V. Saveliev, "The recent development and study of silicon photomultiplier," *Nucl. Instr. Meth. A*, vol. 518, pp. 560–564, 2004.
- [6] D. P. McElroy, V. Saveliev, A. Reznik, and J. A. Rowlands, "Evaluation of silicon photomultipliers: A promising new detector for MR compatible PET," *Nucl. Instr. Meth. A*, vol. 571, pp. 106–109, 2007.
- [7] S. Cova, M. Ghioni, A. Lacaita, C. Samori, and F. Zappa, "Avalanche photodiodes and quenching circuits for single-photon detection," *Appl. Opt.*, vol. 35, no. 12, p. 1956, 1996.
- [8] R. G. W. Brown, K. D. Ridley, and J. G. Rarity, "Characterization of silicon avalanche photodiodes for photon correlation measurements, 1: Passive quenching," *Appl. Opt.*, vol. 25, no. 22, pp. 4122–4126, 1986.
- [9] R. G. W. Brown, R. Jones, J. G. Rarity, and K. D. Ridley, "Characterization of silicon avalanche photodiodes for photon correlation measurements, 2: Active quenching," *Appl. Opt.*, vol. 26, no. 12, pp. 2383–2389, 1987.
- [10] S. J. Buckley, S. J. Bellis, P. Rosinger, and J. C. Jackson, "Fully integrated sub 100 ps photon counting platform," *Proc. SPIE*, vol. 6471, pp. 647116-1–647116-12, 2007.
- [11] J. C. Jackson, A. P. Morrison, D. Phelan, and A. Mathewson, "A novel silicon Geiger-mode avalanche photodiode," in *Proc. IEEE Int. Electron Devices Meeting (IEDM)*, 2002, vol. 32, pp. 797–800.
- [12] S. M. Sze, *Physics of Semiconductor Devices*, 2nd ed. New York: Wiley-Interscience, 1981, p. 751.
- [13] R. J. McIntyre, "On the avalanche initiation probability of avalanche diodes above the breakdown voltage," *IEEE Trans. Electron Devices*, vol. ED-20, no. 7, pp. 637–641, Jul. 1973.
- [14] S. Cova, A. Lacaita, and G. Ripamonti, "Trapping phenomena in avalanche photodiodes on nanosecond scale," *IEEE Electron Device Lett.*, vol. 12, no. 12, pp. 685–687, Dec. 1991.
- [15] J. C. Jackson, D. Phelan, A. P. Morrison, R. M. Redfern, and A. Mathewson, "Characterization of Geiger mode avalanche photodiodes for fluorescence decay measurements," *Proc. SPIE*, vol. 4650, pp. 55–66, 2002.
- [16] V. D. Kovaltchouk, G. J. Lolos, Z. Papandreou, and K. Wolbaum, "Comparison of a silicon photomultiplier to a traditional vacuum photomultiplier," *Nucl. Instr. Meth. A*, vol. 538, pp. 408–415, 2005.
- [17] N. Akil, "A multi-mechanism model for photon generation by silicon junctions in avalanche breakdown," *IEEE Trans. Electron Devices*, vol. 46, no. 5, p. 1022, May 1999.
- [18] A. L. Lacaita, F. Zappa, S. Bigliardi, and M. Manfredi, "On the bremsstrahlung origin of hot-carrier-induced photons in silicon devices," *IEEE Electron Device Lett.*, vol. 40, pp. 577–582, 1993.
- [19] J. G. Rarity, T. E. Wall, K. D. Ridley, P. C. M. Owens, and P. R. Tapster, "Single-photon counting for the 1300–1600-nm range by use of peltier-cooled and passively quenched InGaAs avalanche photodiodes," *Appl. Opt.*, vol. 39, no. 36, pp. 6746–6753, 2000.
- [20] S. M. Sze, *Physics of Semiconductor Devices*, 2nd ed. New York: Wiley-Interscience, 1981, pp. 89–92.

**A. G. Stewart** received the B.Sc. (hons.) degree in physics from the University of Manchester, Manchester, U.K., in 1998, the M.Sc. degree in optoelectronic and laser devices from St. Andrews University, St. Andrews, U.K., in 1999, and the Ph.D. from Heriot-Watt University, Edinburgh, U.K., in 2003.

In 2003, he joined the Engineering Department, Cambridge University, Cambridge, U.K., where he was engaged in research on the application of semicon-

ductor devices to the detection of biological interactions. In 2005, he joined SensL, Cork, Ireland, as a Design Engineer working on the design, modeling and characterization of silicon photon counting detectors and silicon photomultipliers.

Dr. Stewart is a member of the Institute of Physics.

**V. Saveliev** graduated in physics and received the Ph.D. degree from the Moscow Physics and Engineering Institute (State University), Moscow, Russia, in 1974 and 1979, respectively.

In 1979, he joined the Department of Elementary Particle Physics, Moscow Physics and Engineering Institute (State University), where he was engaged in research in experimental high-energy physics and semiconductor radiation detectors. In 1980, he was appointed Assistant Professor of the same department and in 2002, he was appointed Professor at the Department of Applied Mathematics, Obninsk State University, Obninsk, Russia. His research interests include mathematical simulation in experimental high-energy physics and semiconductor technology for radiation detectors.

**S. J. Bellis** received the B.Sc. (hons.) degree in electronic engineering and the Ph.D. degree from the University of Wales, Bangor, U.K., in 1991 and 1996, respectively.

In 1996, he joined University College Cork, Ireland, as a Postdoctoral Researcher. In 1997, he joined the Tyndall National Institute, Cork, Ireland, as a Research Engineer. In 2001, he joined the Ambient Electronic Systems Group at Tyndall. In March 2005, he joined SensL, Cork, Ireland, as Senior Design Engineer to develop instrumentation for solid-state photon counting.

**D. J. Herbert** received the B.Sc. (hons) degree in physics with space science and the Ph.D. in physics from the University of Southampton, Southampton, U.K., in 1998 and 2002, respectively.

In 2005, she held a postdoctoral position at the Università di Pisa, Pisa, Italy, carrying out research on high-resolution gamma cameras for dedicated PET systems and in the use of the Silicon Photomultiplier (SPM) for readout of scintillators. She joined SensL, Cork, Ireland, in 2006 to continue her work with SPM.

**P. J. Hughes** received the B.Sc. (hons) degree from the Department of Physics, Essex University, Essex, U.K., and the Ph.D. degree from the Department of Electronic Engineering, University of Surrey, Surrey, U.K., in 1995.

In 2002, he held the post of Senior Research Scientist at the Tyndall National Institute, Ireland, and in 2004 he was Photonics Strand Leader for the National Centre of Excellence in Telecommunication Research (CTRV). In 2005, he joined SensL, Cork, Ireland, as Product Manager for the company's Silicon Photomultiplier product line. His research interests include optoelectronic devices, MEMS, and optical interconnect & packaging.

Dr. Hughes is a Chartered Physicist of the Institute of Physics.

**J. C. Jackson** received the B.Sc. and M.Sc. degrees in electrical engineering from Clemson University, Clemson, SC, and the Ph.D. degree in microelectronic engineering from University College, Cork, Ireland.

In 2002, he founded Photon Detection Systems to commercialize technology in low light detection. In 2004, he co-founded SensL, Cork, Ireland, to develop silicon single photon counting detectors, silicon photomultipliers, and photon counting/timing cameras. He is currently serving as Chief Technology Officer at SensL.